Transport and Telecommunication, 2015, volume 16, no. 2, 158–166
Transport and Telecommunication Institute, Lomonosova 1, Riga, LV-1019, Latvia
DOI 10.1515/ttj-2015-0015

CYCLIC FRACTURE TOUGHNESS OF RAILWAY AXLE AND MECHANISMS OF ITS FATIGUE FRACTURE

Andriy Sorochak [1]***, Pavlo Maruschak*** [2]***, Olegas Prentkovskis*** [3]

[1] *Ternopil Ivan Pul'uj National Technical University*
Rus'ka str. 56, 46001 Ternopil, Ukraine
E-mail: sorochak_a@mail.ua

[2] *Ternopil Ivan Pul'uj National Technical University*
Rus'ka str. 56, 46001 Ternopil, Ukraine
E-mail: maruschak.tu.edu@gmail.com

[3] *Vilnius Gediminas Technical University*
Plytines g. 27, LT-10105 Vilnius, Lithuania
E-mail: olegas.prentkovskis@vgtu.lt

The main regularities in fatigue fracture of the railway axle material – the OSL steel – are found in this paper. Micromechanisms of fatigue crack propagation are described and systematized, and a physical-mechanical interpretation of the relief morphology at different stages of crack propagation is proposed for fatigue cracks in specimens cut out of the surface, internal and central layers of the axle.

Keywords: fatigue, fracture, mechanisms of damage, stress-strain state, railway axle

1. Introduction

During the analysis of the effect of the loading cycle stress ratio on fracture toughness of materials, an increase in the loading cycle stress ratio in case of positive asymmetries causes a decrease in the stress amplitude necessary to ensure a certain crack propagation rate (Carlson and Kardomateas, 1994). However, in case of negative asymmetries, the crack propagation mechanism is more complex, and the results of previous years indicate that it is necessary to consider the effect of compressive stresses on the fatigue crack propagation mechanism.

It is known that the effect of the loading cycle stress ratio is connected with closure of the fatigue crack tip during its growth (Silva, 2005; Xiong *et al*., 2008; Zhang *et al*., 2010). In addition, during the construction of a kinetic diagram of fatigue fracture, the negative part of the loading cycle is, as a rule, neglected (ASTM E647-08e1, 2008). However, if we analyze the fatigue crack growth process at the macro- and meso- levels, the process of the crack face closure can influence the stress-strain state at the crack tip and change micromechanisms of its propagation (Plekhov *et al*., 2007; Panin *et al*., 2011). Moreover, it is established that in case of significant negative asymmetries the crack growth can be speeded up. In addition, there is certain ambiguousness in the influence of negative asymmetries of the loading cycle on the fatigue crack growth and fractographic parameters of the fracture surface. On the one hand, compressive strains cause crushing of the relief elements, however, the relief formations make impossible full closure of the crack tip, which might cause an increase in its growth rate. In previous papers, the authors used scanning electron microscopy, optical microscopy and a number of metallographic approaches to study the fatigue crack propagation mechanisms (Maruschak *et al*., 2013). This work allows using the well-established methods for the assessment of the fatigue crack propagation kinetics in the railway axle material at different distances from the surface, i.e. taking into account the technological and operating influence, which affects fracture toughness of the service-exposed steel (Varfolomeev *et al*., 2011; Yasniy *et al*., 2013).

The purpose of this work is to investigate the cyclic fracture toughness of the railway axle steel and the mechanisms of its fatigue failure in case of different loading cycle asymmetries.

2. Materials and research technique

Fracture toughness of the locomotive wheel-set axle material – the OSL steel – was determined using prismatic specimens with the central crack of $155 \times 25 \times 5$ mm. Specimens were cut in the longitudinal direction at a distance of 20, 50 and 81 mm from the center of the axle.

We designate specimens depending on their distance from the axle center as follows, Fig. 1:

- specimens cut at a distance of 20 mm (A);
- specimens cut at a distance of 50 mm (B);
- specimens cut at a distance of 81 mm (C).

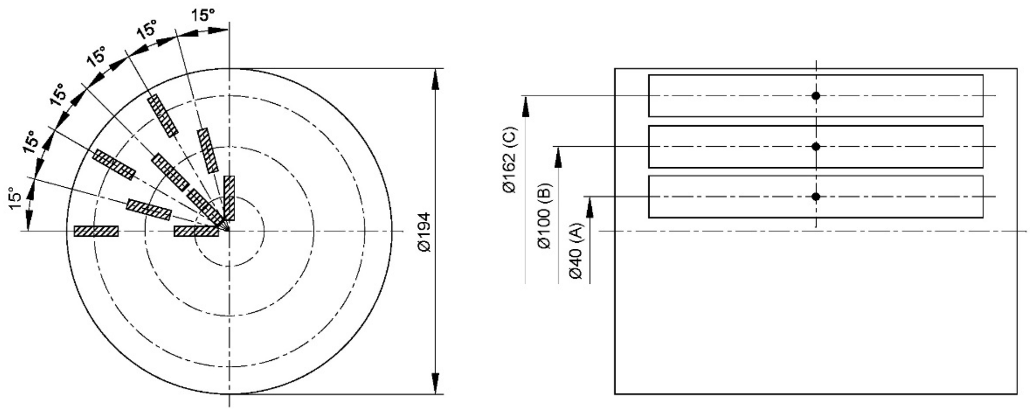

Figure 1. Scheme of cutting specimens with a central opening from locomotive axle at different distances from its surface (GOST 31334-2007)

The stress intensity factor for the prismatic specimen with the central crack was calculated from the following formula (ASTM E647-08e1, 2008):

$$K = \sigma \cdot \sqrt{\pi \cdot a} \cdot Y;$$

$$Y = \left(1 - 0.025 \cdot \left(\frac{2 \cdot a}{W}\right)^2 + 0.06\left(\frac{2 \cdot a}{W}\right)^4\right) \cdot \left(\sec\left(\frac{\pi \cdot a}{W}\right)\right)^{0.5},$$

where K is stress intensity factor; a is the half-length of the crack; W is the specimen width.

In addition, the range of the stress intensity factor was calculated following the recommendation of standard (ASTM E647-08e1, 2008):

$$\Delta K = \begin{cases} (1 - R) \cdot K_{\max} & \text{for } R \geq 0; \\ K_{\max} & \text{for } R < 0, \end{cases}$$

where K_{max} is the maximum stress intensity factor in the loading cycle; R is loading cycle stress ratio coefficient.

The experimental investigations were carried out under uniaxial tension with the loading cycle stress ratio coefficient $R = -1$ and $R = 0$. The loading frequency was $f = 10$ Hz, the form of the cycle was sinusoidal. The investigations were conducted at a room temperature using the STM-100 servo-hydraulic test setup with computer control and data logging. This setup allows monitoring the loading of test specimens using one channel with a simultaneous recording of measurements by six measurement channels using special software. The optical system based on the MBS-10 metallographic microscope was used for measuring the crack length.

Fracture surfaces with different SIFs were investigated on the REM-106I raster electron microscope in the secondary electrons mode with the following parameters: cathode voltage – 20–30 kV, current – 160–200 μA, focal distance – 9–15 mm. Specialized software KAPPA ImageBase was used for the quantitative analysis of the obtained images.

3. Macroregularities

Studying the effect of the loading stress ratio on the fatigue crack growth kinetics allows for a more precise definition of the residual life of railway axles and formulation of the physical background of diagnostics of the technical condition of the structure. It should be noted that under all the test temperatures the regularities of the fatigue failure of the OSL steel have the “classical view”, Fig. 2.

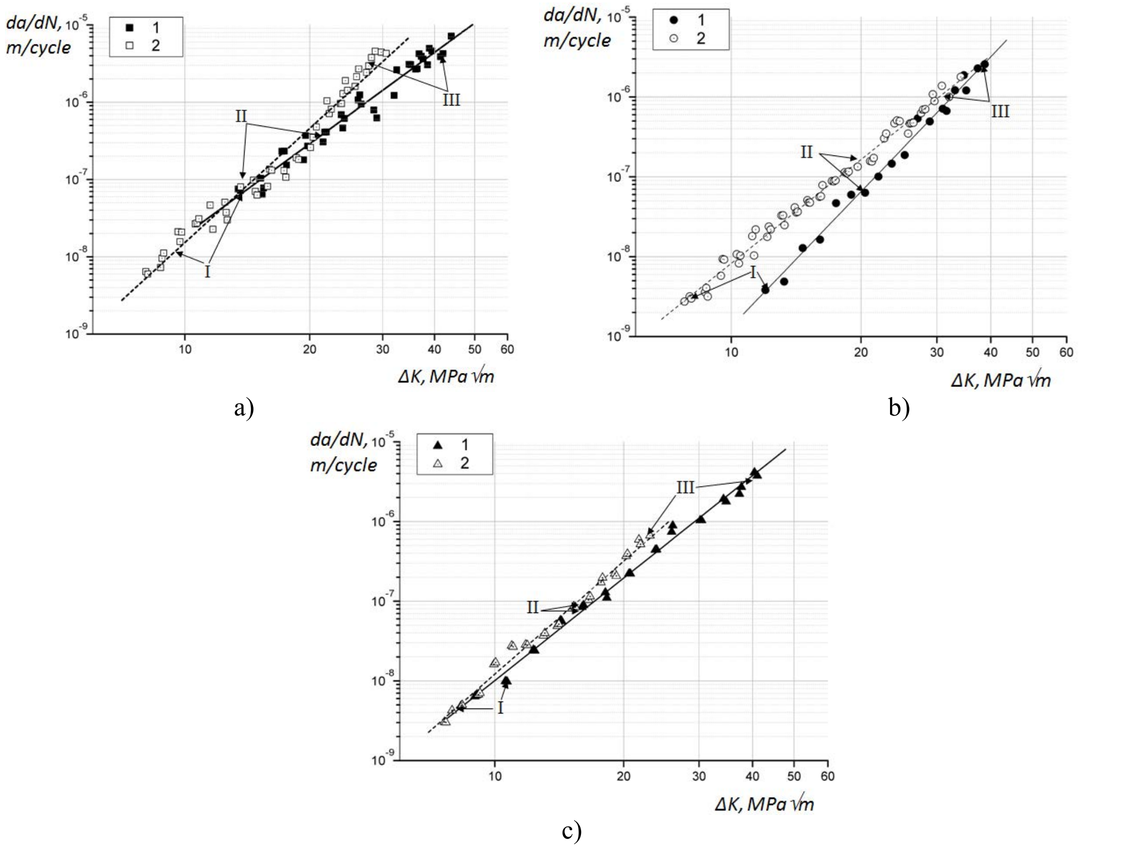

Figure 2. Kinetic diagrams of fatigue fracture of railway axle material cut at different distances from the axle center: a – 20 mm (A); b – 50 mm (B); c – 81 mm (C), under loading cycle stress ratio: 1 – $R = 0$; 2 – $R = -1$; I–III – points of fractographic analysis

Cutting zone A. The results of the investigations into the fatigue crack growth rate (FCGR) in coordinates *da/dN–ΔK* are presented in Fig. 2a. Arrows indicate the moments of conducting the fractographic microanalysis. In this case, the slope of the diagram describes the damage accumulation rate. It is found that the loading cycle stress ratio $R = 0$ and cyclic fracture toughness is 2–4 times lower than the stress ratio $R = -1$ within the SIF range from 20 to 35 MPa√m.

Cutting zone B. The results of the investigations into the FCGR in coordinates *da/dN–ΔK* are presented in Fig. 2b. It is established that at low values ΔK = 10 MPa√m under the loading cycle stress ratio $R = 0$, the cyclic fracture toughness is 8 times higher than at the stress ratio $R = -1$. However, this difference decreases gradually, and at ΔK = 30 MPa√m, the FCGR is the same for both asymmetries.

Cutting zone C. The results of the investigations into the fatigue crack growth rate (FCGR) in coordinates *da/dN–ΔK* are presented in Fig. 2c. The FCGR at ΔK = 10 MPa√m is practically the same, however, with an increase in the SIF excursion, the difference between the above values increases, and already at ΔK = 25 MPa√m the cyclic fracture toughness of the OSL steel under the loading cycle stress ratio $R = 0$ is 2–3 times lower than at the stress ratio $R = -1$.

The above regularities indicate the ambiguous effect of the loading cycle stress ratio on the material cut out of various sections of the axle. In our opinion, this can be due to the effect of the structural and mechanical peculiarities of the OSL steel, when the cyclic fracture toughness depends in a complex way on the size and structure of the pearlitic grains and the nature of fracture of the pearlitic structures. In previous works, the complex character of the effect of differences in the dispersion, morphology and the cementite damage was found, as well as the effect of the dislocation hardening mechanisms of the ferritic component on the fracture mechanisms of the ferritic-pearlitic steels (Maruschak *et al.*, 2013).

4. Effect of loading stress ratio on micromechanisms of fracture of the OSL steel

The qualitative and quantitative morphological analysis of the peculiarities of the fatigue crack propagation in the railway axle steel is performed.

Specimens A.

Load ratio *R* = 0. Fracture surface is formed by the ductile-brittle mechanism, Fig. 3a,b. Disoriented relief formations are noticeable on the fracture surface (*section I*). However, typical fatigue striations with quite a large step of 1 μm were observed on individual surfaces.

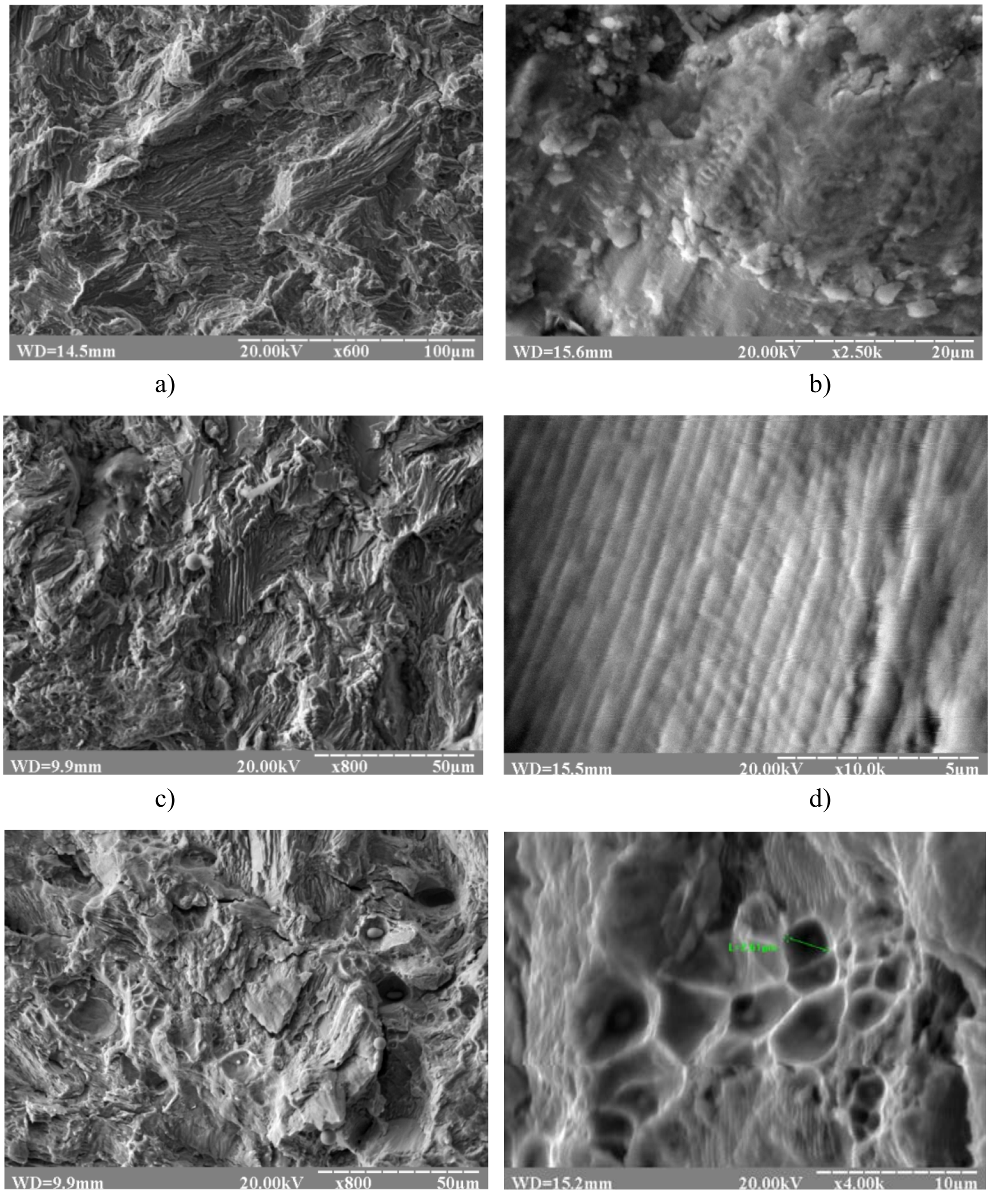

a) b)

c) d)

e) f)

Figure 3. Micromechanisms of fatigue crack growth in the OSL steel in case of loading cycle stress ratio $R = 0$ (a–e) and $R = -1$ (points of fractographic analysis are shown in Fig. 2a)

The specimen surface (*section II*) is fragmented heavily, therefore, we can speak only about the macrodirection of crack propagation. In addition, there is no general crack propagation area at the macrolevel. The crack front moved from one octahedral area to another, forming terraces and steps, due to which the terrace acquired a curvilinear trajectory, Fig. 3c. It should be noted that due to a complex stress state in the cyclic plastic zone in front of the crack tip, the direction of the lines of fatigue striations differ significantly in the neighboring structural elements, Fig. 3c, since the fatigue crack propagates locally in the direction with the minimal fracture energy (Maruschak *et al*., 2012; Shaniavski *et al*., 2004).

The fatigue crack growth within *section III* determined the transition of deformation mechanisms to the macroscale level and an increase in the FCR rate. An increase in the crack length had practically no effect on the crack propagation mechanism, only the share of ductile separation was increasing, and the striation mechanism disappeared gradually, Fig. 3d. At high propagation rates and within the zone of static rupture of the specimen material, a typical dimple failure was observed, and some inclusions of the circular and oblong shape were noticeable at the bottom of individual dimples, Fig. 3e. The crack growth mechanisms acquire ductile character, which preconditions the increased strain localization and the effect of rotational plasticity. An increase in the level of plastic deformation causes the localization of plastic strains in the vicinity of the microstructure elements: inclusions, subgrain boundaries, microfailure and separation of coherent links between inclusions and the matrix, which explains the formation of the local zones of dimple separation. In case of a "long" crack, local "tears" of the specimen material were observed at the ends of secondary microcracks, the formation of which was accompanied by shear strains (Shanyavskiy, 2013). Crack propagation is accompanied by the activation of secondary cracking and branching of the main crack.

With an increase in the crack length, the influence of inclusions and disperse particles on the fatigue crack propagation mechanisms increases. Large separation dimples, which were formed due to separation of inclusions from the matrix, are noticeable on the fracture surface, Fig. 3f. Significant strains along the body and within the grains facilitate the development of the plastic zone at the crack tip, thus speeding up failure processes and causing the formation of individual microcracks, which then coalesce with the main crack. The traces of such coalescence create scars on the fracture surface.

Load ratio $R = -1$. Failure of the material took place by the mechanisms similar to stress ratio $R = 0$. The crack propagated in the non-uniform manner, fracture had a ductile-brittle character, Fig. 3a,b. It should be noted that the front of the fatigue crack penetration (*section I*) is fragmented heavily, it is covered with terraces and "steps". This indicates the activation of shear processes within the pearlitic grains (Maruschak *et al.*, 2013; Shanyavskiy and Burchenkova, 2013).

The fracture morphology (*section II*) indicates strength and plasticity of the material. The fracture surface is formed by the "corrugated" relief, Fig. 3c, which is located at different angles relative to the crack propagation direction, the striations are located on the surfaces of terraces, Fig. 3d. The crack front propagated in the non-uniform manner, which indicates strain localization within certain sections of the materials.

Well-developed sections of crushing of the fracture surface were observed, Fig. 3e, which indicates the crack closure. However, like in the previous case, the crack propagated by the striation mechanism, which then changed into the mixed one and had a ductile character within the pre-failure zone (*section III*), Fig. 3f.

Specimens B.

$R = 0$. Smoothed out facets with traces of the intragranular multiple sliding were observed (*section I*). In addition, stepwise disoriented relief formations covered with fatigue striations were found, Fig. 4a. However, even within individual facets, the orientation of striations was not permanent. The facets of the intragranular failure are covered with striations, which alternate with the split pearlitic grains, whose failure took place by means of spalling across the crack of the cementite plate, Fig. 4b. Moreover, fatigue striations are the only acting mechanism of crack propagation (*section II*). With an increase in the stress intensity factor, the facets lose the expressed ductile-brittle manifestations and acquire the "smoothed-out" shape, which, in our opinion, is the confirmation of a more pronounced manifestation of plastic deformation of the material (dimensions of the plastic zone) at the crack tip, and an increased share of ductile separation on the fracture surface of the OSL steel (*section III*), Fig. 4e.

$R = -1$. A decrease in the fatigue crack propagation rate at the loading cycle stress ratio $R = -1$ compared to R = 0 is due to the crack branching processes in the pearlitic grains and local blunting of the crack tip in the ferritic component (*section I*), Fig. 4c. Moreover, the formation of facets and separation of the pearlitic grains was observed, Fig. 4d (*section II*). Therefore, an increase in the active loading time during the specimen loading did not ensure the accumulation of structural damage, however, it contributed to the activation of the relaxation processes in the material and, correspondingly, a decrease in the FCG rate. It should be noted that the size of microbranching was less than that of the ferritic grains, which hampered the crack propagation during its growth through the pearlitic grains. Moreover, the fragmentation and milling of the cementite plates took place in the pearlitic grains.

However, with an increase in the size of the pearlitic zone, greater volumes of the material become involved in the deformation process, which preconditions an increase in the intensity of the structural defect accumulation in the grain conglomerates (*section III*). In addition, the crack propagation mechanisms at different asymmetries become more similar, which is depicted on the kinetic curve (Wawszczak and Kurzydłowski, 2009).

Specimens C

During fractographic investigations it was found that the fracture relief morphology of the specimens tested at different loading asymmetries is similar (*sections I* and *II*). The influence of the pearlitic colonies on the fatigue crack propagation kinetics was observed, which was depicted in the presence of the fatigue and ductile-brittle crack propagation sections on the surface, Fig. 5a. In our opinion, the pearlitic colonies, which are situated on the trajectory of the fatigue crack tip, cause the relaxation effects, Fig. 5a. However, an increase in the SIF causes an increase in the share of the ductile propagation of the crack, in particular, the dimple component, which causes a decrease in the size of the separation facets and the appearance of the ductile separation dimples (*section I, II*).

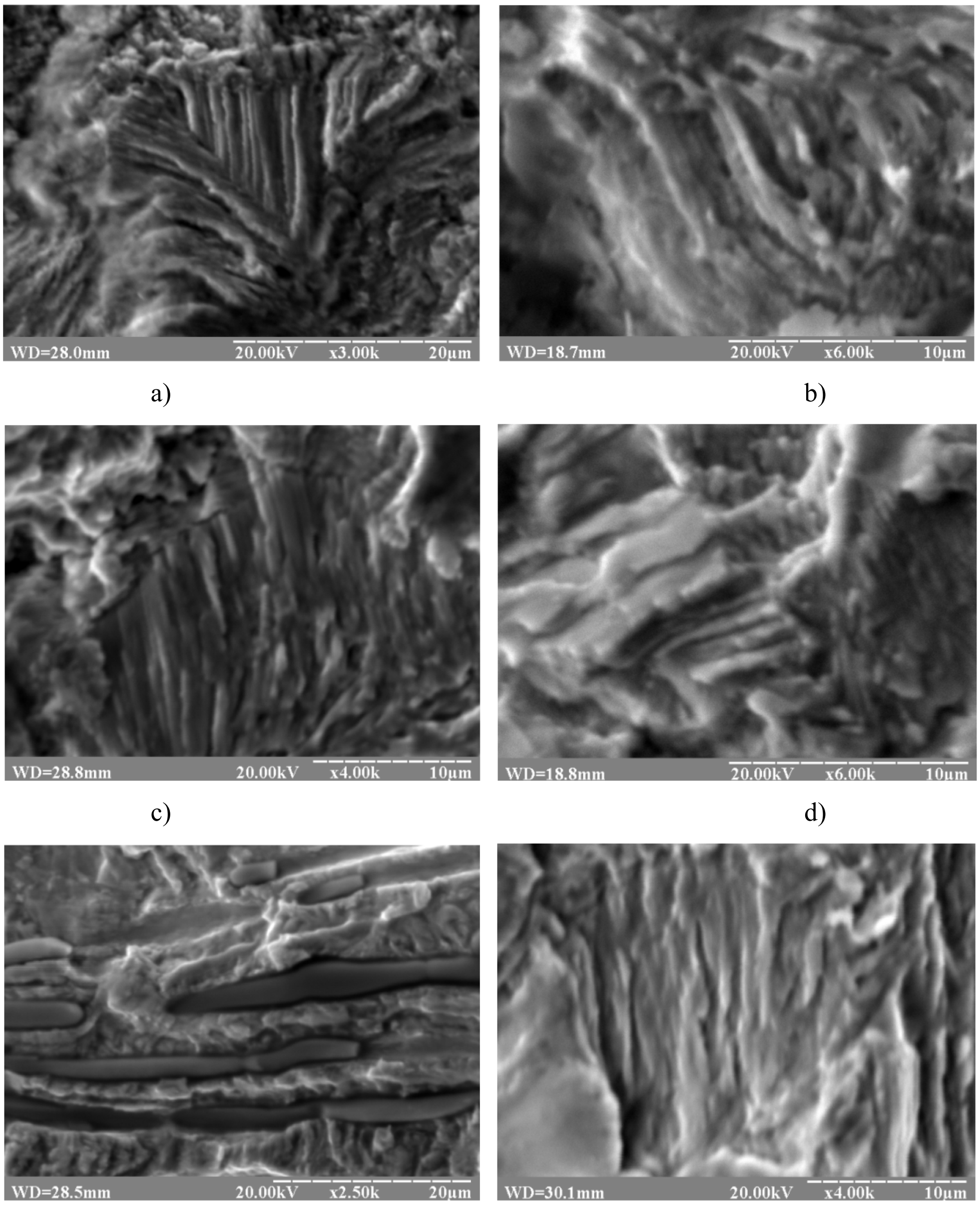

Figure 4. Micromechanisms of fatigue crack growth in the OSL steel in case of loading cycle stress ratio $R = 0$ (a–d) and $R = -1$

The fracture surface consists of numerous terraces decorated with the fragmentarily located series of striations, Fig. 5b. However, there are certain differences in the view of the terraces and “steps”, which are a little bigger than the stress ratio $R = -1$. At the same time, their geometry indicates that during crack propagation they created the local relaxation sections. This causes a decrease in the microrate of crack propagation (step of fatigue striations) on individual sections of the crack front, which was observed on the fracture surface.

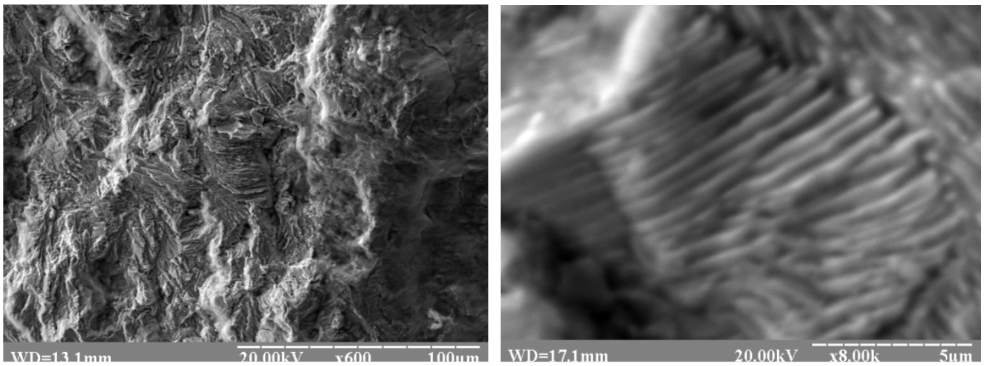

a) b)

Figure 5. Micromechanisms of fatigue crack growth in the OSL steel in case of loading cycle stress ratio $R = 0$

5. Influence of structural nonuniformity of material on its fracture toughness

The analysis of interrelation between the macro- and micromechanisms of fracture allows for a partial understanding of the crack closure effect at the stress ratio $R = -1$ on the ferritic-pearlitic steel OSL. The crack closure in case of compressive loading is not taken into account during the computation of the SIF excursion. However, it exists at the physical level, and its influence on the micromechanisms of crack propagation must be taken into account, Fig. 6.

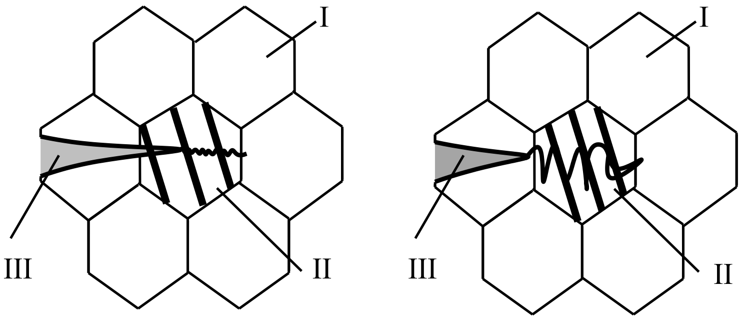

a) b)

Figure 6. Physical regularities in crack propagation in specimens A, C (a) and B (b);
I – ferritic grain; II – pearlitic grain; III – crack

Based on the results of the fractographic investigations it was found that within the specimens cut out of the A, C zone, the fatigue crack propagation scheme was implemented, Fig. 6a. However, within the specimens cut out of the B zone, the mixed mechanism of crack propagation (fatigue + quasi-spalling) was observed, Fig. 6b.

The influence of the negative asymmetries during the fatigue crack propagation caused two main effects (Larijani *et al*., 2014; Elwazri *et al*., 2005) that were observed in our case:

- crushing of irregularities and an increase in the crack opening range;
- lack of crushing – a decrease in the fatigue crack propagation rate was observed.

Moreover, there are differences within the section of pre-failure and quasi-static rupture. For the specimen with $R = 0$, some empty dimples were found, whose shape is close to the particles of the disperse inclusions torn from the material. For the material tested at $R = -1$, "large" inclusions were found, which are located in the cavities that were formed around them during plastic deformation. These particles are one of the sources of the material anisotropy (Elwazri *et al*., 2005; Černý and Linhart, 2013). While creating the sections of the local plastic strains, they impede the passage of the crack front through them. As a result, the crack front "crushes" and gets covered with the disoriented terraces, Fig. 6b. Based on the experimental results, the values of the C coefficients and the n degree of the Paris equation for the loading cycle stress ratio $R = 0$ and $R = -1$ are found, Table 1.

The results obtained allow stating that the macro- and micro-regularities of the fatigue crack propagation in the wheel-set axle material depend on the material structure formed during the technological process of manufacturing (Levchenko *et al*., 2010). At the same time, the effect of cyclic loading and microlocalization of deformation processes in the material can be evaluated from the morphological peculiarities of fatigue fracture, Table 2.

Table 1. Cyclic fracture toughness parameters of the OSL steel used in wheel-set axle

R	Cutting distance	C, $\frac{m/cycle}{\left(MPa\sqrt{m}\right)^n}$	n
0	A	$2.26 \cdot 10^{-12}$	3.923
	B	$3.22 \cdot 10^{-15}$	5.615
	C	$5.34 \cdot 10^{-13}$	4.273
–1	A	$1.86 \cdot 10^{-13}$	4.911
	B	$3.87 \cdot 10^{-13}$	4.325
	C	$2.35 \cdot 10^{-13}$	4.710

Table 2. Generalized peculiarities of fatigue crack propagation in the OSL steel

R	Main fracture mechanisms of specimens cut out of different zones of cutting		
	A	B	C
0	Striation mechanism (clear-cut ordered striations); Facets of spalling; Separation dimples.	Facets of spalling; Facets of failure of pearlitic grains; Pseudo-striations.	Striation mechanism (clear-cut ordered striations).
–1	Striation mechanism (clear-cut ordered striations); Large facets of spalling decorated with striations.	Facets of spalling of pearlitic grains; Pseudo-striations; Fracture has a ductile-brittle view similar to quasi-static failure.	Striation mechanism (clear-cut ordered striations).

6. Conclusions

Using the approaches of fracture mechanics and physical mesomechanics the graded nature of the fatigue crack growth in specimens from the OSL steel with the central opening at the loading cycle stress ratio R = 0 and R = -1 is investigated. The fatigue crack growth kinetics at different stages of its propagation are found and described quantitatively.

For the specimens cut out of the center of the axle (A) at the loading cycle stress ratio R = 0, the cyclic fracture toughness is 2–4 times lower than at the stress ratio R = –1within the SIF range from 20 to 35 MPa√m. The cyclic fracture toughness of the specimens cut out of the middle layer of the axle (B) is 2–8 times higher at R = 0 than at R = –1, which is connected with a change of fracture mechanisms. If in the previous case the prevailing mechanism was the fatigue intragranular failure, in this case a significant effect was due to spalling of the pearlitic grains, which caused the crack branching. For the specimens cut out of the axle surface (C), the cyclic fracture toughness of the OSL steel at the stress ratio R = 0 is 1.5–2.5 times lower than at the stress ratio R = –1.

The microregularities of the fatigue crack propagation in the OSL steel are analyzed and generalized. At low SIF values, the specimen fracture surface is formed from terraces with the striation-like relief, and the share of the ductile (dimple) component increases with an increase in the crack length. The pre-failure zone of the specimen has features of the ductile failure followed by separation of inclusions from the material matrix and the formation of dimple relief.

References

1. ASTM E647-08e1. (2008) Standard Test Method for Measurement of Fatigue Crack Growth Rates.
2. Carlson, R. L., Kardomateas, G. A. (1994) Effects of compressive load excursions on fatigue crack growth. *International Journal of Fatigue*, 16(2), 141–146. DOI: 10.1016/0142-1123(94)90104-X
3. Černý, I., Linhart, V. (2013) Effects of different microstructure on resistance of EA4T railway axle steel of equal strength to fatigue crack growth. *Key Engineering Materials*, 592–593, 631–634. DOI:10.4028/www.scientific.net/KEM.592-593.631

4. Elwazri, A. M., Wanjara, P., Yue, S. (2005) The effect of microstructural characteristics of pearlite on the mechanical properties of hypereutectoid steel. *Materials Science and Engineering: A*, 404 (1–2), 91–98. DOI:10.1016/j.msea.2005.05.051
5. GOST 31334-2007. Osi dlya podvizhnogo sostava zheleznyh dorog kolei 1520 mm. Tehnicheskie usloviya [Axles for rolling stock of 1520 mm gauge railways. Specifications]. (in Russian).
6. Larijani, N., Brouzoulis, J., Schilke, M., Ekh, M. (2014) The effect of anisotropy on crack propagation in pearlitic rail steel. *Wear*, 314(1–2), 57–68. DOI:10.1016/j.wear.2013.11.034
7. Levchenko, G. V., Dyomina, E. G., Nefedyeva, E. E., Buga, I. D., Antonov, Yu. G., Medinskiy, G. A. (2010) Effect of billet strained condition on microstructure homogeneity of railway axles. *Metallurgical and Mining Industry*, 2(3), 207–214.
8. Maruschak, P. O., Baran, D. Ya., Sorochak, A. P., Bishchak, R. T., Yasnii, V. P. (2012) Cyclic crack resistance and micromechanisms of fracture of steel 25Kh1M1F. *Strength of Materials*, 44(4), 410–418. DOI:10.1007/s11223-012-9395-0
9. Maruschak, P. O., Sorochak, A. P., Menou, A., Maruschak, O. V. (2013) Regularities in macro- and micromechanisms of fatigue crack growth in a bimetal of continuous caster rolls. *Case Studies in Engineering Failure Analysis*, 1(2), 165–170. DOI:10.1016/j.csefa.2013.05.003
10. Panin, V. E., Elsukova, T. F., Popkova, Yu. F. (2011) Stages of multiscale fatigue cracking as a nonlinear rotational autowave process. *Physical Mesomechanics*, 14(3–4), 112–123. DOI:10.1016/j.physme.2011.08.003
11. Plekhov, O. A., Saintier, N., Palin-Luc, T., Uvarov, S. V., Naimark, O. B. (2007) Theoretical analysis, infrared and structural investigations of energy dissipation in metals under cyclic loading. *Materials Science and Engineering: A*, 462(1–2), 367–369. DOI:10.1016/j.msea.2006.02.462
12. Shanyavskiy, A. A. (2013) Mechanisms and modeling of subsurface fatigue cracking in metals. *Engineering Fracture Mechanics*, 110, 350–363. DOI:10.1016/j.engfracmech.2013.05.013
13. Shaniavski, A. A., Artamonov, M. A. (2004) Fractal dimensions for fatigue fracture surfaces performed on micro- and meso-scale levels. *International Journal of Fracture*, 128(1–4), 309–314. DOI:10.1023/B:FRAC.0000040994.96074.bf
14. Shanyavskiy, A. A., Burchenkova, L. M. (2013) Mechanism for fatigue striations as formed under variable negative R-ratio in Al-based structural alloys. *International Journal of Fatigue*, 50, 47–56. DOI:10.1016/j.ijfatigue.2012.04.006
15. Silva, F. S. (2005) The importance of compressive stresses on fatigue crack propagation rate. *International Journal of Fatigue*, 27(10–12), 1441–1452. DOI:10.1016/j.ijfatigue.2005.07.003
16. Varfolomeev, I., Luke, M., Burdack, M. (2011) Effect of specimen geometry on fatigue crack growth rates for the railway axle material EA4T. *Engineering Fracture Mechanics*, 78(5), 742–753. DOI:10.1016/j.engfracmech.2010.11.011
17. Wawszczak, J., Kurzydłowski, K. J. (2009) Grain size correlation with the geometry of fracture surface profiles in polycrystalline iron by a continuous wavelet transformation method. *Materials Characterization*, 60(10), 1180–1184. DOI:10.1016/j.matchar.2009.02.014
18. Xiong, Y., Katsuta, J., Kawano, K., Sakiyama, T. (2008) Examination of fatigue crack driving force parameter. *Fatigue & Fracture of Engineering Materials & Structures*, 31(9), 754–765. DOI:10.1111/j.1460-2695.2008.01261.x
19. Yasniy, O., Lapusta, Y., Pyndus, Y., Sorochak, A., Yasniy, V. (2013) Assessment of lifetime of railway axle. *International Journal of Fatigue*, 50, 40–46. DOI:10.1016/j.ijfatigue.2012.04.008
20. Zhang, J., He, X. D., Sha, Y., Du, S. Y. (2010) The compressive stress effect on fatigue crack growth under tension–compression loading. *International Journal of Fatigue*, 32(2), 361–367. DOI:10.1016/j.ijfatigue.2009.07.008